JACS JOURNAL OF THE AMERICAN CHEMICAL SOCIETY

Communication

Cite This: J. Am. Chem. Soc. 2018, 140, 10416−10420

pubs.acs.org/JACS

Intrinsic Properties of Single Graphene Nanoribbons in Solution: Synthetic and Spectroscopic Studies

Yinjuan Huang,[†,¶] Fugui Xu,[†,¶] Lucia Ganzer,[‡] Franco V. A. Camargo,[‡] Tetsuhiko Nagahara,[‡,§] Joan Teyssandier,[∥] Hans Van Gorp,[∥] Kristoffer Basse,[⊥] Lasse Arnt Straasø,[⊥] Vaiva Nagyte,[#] Cinzia Casiraghi,[#] Michael Ryan Hansen,[▽] Steven De Feyter,[∥] Deyue Yan,[†] Klaus Müllen,[○] Xinliang Feng,[◆] Giulio Cerullo,*[,‡] and Yiyong Mai*[,†]

[†]School of Chemistry and Chemical Engineering, Shanghai Jiao Tong University, 800 Dongchuan RD, Shanghai 200240, China

[‡]IFN-CNR, Dipartimento di Fisica, Piazza L. da Vinci 32, 20133 Milano, Italy

[§]Department of Chemistry and Materials Technology, Kyoto Institute of Technology, 606-8585 Kyoto, Japan

[∥]Division of Molecular Imaging and Photonics, Department of Chemistry, KU Leuven, Celestijnenlaan, 200 F, B-3001 Leuven, Belgium

[⊥]Interdisciplinary Nanoscience Center, Aarhus University, Gustav Wieds Vej 14, DK-8000 Aarhus C, Denmark

[#]School of Chemistry, University of Manchester, Oxford Road, Manchester M139PL, United Kingdom

[▽]Institute of Physical Chemistry, Westfälische Wilhelms-Universität Münster, Corrensstr. 28/30, D-48149 Münster, Germany

[○]Max Planck Institute for Polymer Research, Ackermannweg 10, 55128 Mainz, Germany

[◆]Department of Chemistry and Food Chemistry, Technische Universität Dresden, Mommsenstrasse 4, 01062 Dresden, Germany

Supporting Information

ABSTRACT: We report a novel type of structurally defined graphene nanoribbons (GNRs) with uniform width of 1.7 nm and average length up to 58 nm. These GNRs are decorated with pending Diels−Alder cycloadducts of anthracenyl units and *N*-*n*-hexadecyl maleimide. The resultant bulky side groups on GNRs afford excellent dispersibility with concentrations of up to 5 mg mL^{-1} in many organic solvents such as tetrahydrofuran (THF), two orders of magnitude higher than the previously reported GNRs. Multiple spectroscopic studies confirm that dilute dispersions in THF (<0.1 mg mL^{-1}) consist mainly of nonaggregated ribbons, exhibiting near-infrared emission with high quantum yield (9.1%) and long lifetime (8.7 ns). This unprecedented dispersibility allows resolving in real-time ultrafast excited-state dynamics of the GNRs, which displays features of small isolated molecules in solution. This study achieves a breakthrough in the dispersion of GNRs, which opens the door for unveiling obstructed GNR-based physical properties and potential applications.

Structurally defined graphene nanoribbons (GNRs) have attracted increasing interest due to their tunable optical, electronic, and magnetic properties by tailoring their width and/or edge structures.[1−18] Two "bottom-up" strategies, including surface-assisted[1−7] and solution-based organic synthesis,[9−17] were developed for GNRs. In contrast to the surface-mediated method, the solution synthesis shows significant advantages in large-scale preparation of liquid-phase-dispersible GNRs.[9−17] However, controlling the physical properties of GNRs, such as optical bandgap and carrier mobility, will be only possible if individual GNRs can be achieved. Otherwise, aggregation effects, which could so far never be excluded, would obscure their intrinsic physical properties.[10−17]

Here, we demonstrate the solution synthesis of a new type of GNRs (hereafter GNR-AHM) with a uniform width of 1.7 nm and average length up to 58 nm, which are decorated with pending Diels−Alder cycloadducts of anthracenyl units and *N*-*n*-hexadecyl maleimide (AHM) (Scheme 1). The AHM side

Scheme 1. Synthesis of GNR-AHM[a]

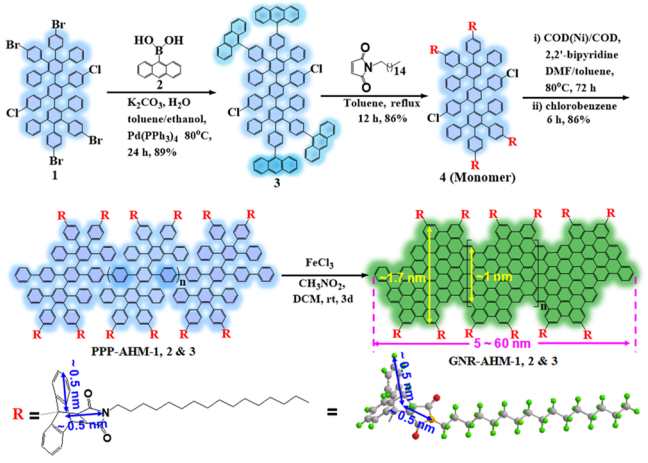

[a]The bulky AHM group size is determined by Chem3D. GNR-AHM-1, 2, and 3 possess average lengths of ca. 6, 11, and 58 nm, respectively.

Received: June 8, 2018
Published: August 7, 2018

DOI: 10.1021/jacs.8b06028
J. Am. Chem. Soc. 2018, 140, 10416−10420

groups have radius of ~0.5 nm, which is larger than the interlayer spacing of graphite (~0.34 nm),[19−21] effectively hindering the $\pi-\pi$ stacking (Scheme S1). GNR-AHMs show unprecedented dispersibility in many organic solvents (e.g., tetrahydrofuran, THF) with concentrations of up to 5 mg mL^{-1} (*for GNR backbone excluding AHM unless otherwise mentioned*). Atomic force microscopy (AFM) analysis of GNR-AHM deposited on graphite substrate shows a periodic self-assembled monolayer structure with a lateral side-by-side alignment of single ribbons. Dynamic light scattering (DLS) and steady state and transient absorption (TA) spectroscopies suggest a single-ribbon feature of the GNRs in dilute dispersions (e.g., <0.1 mg mL^{-1} in THF), thus allowing to unravel the photophysical properties of isolated GNRs in liquid phase.

The chemical synthesis of GNR-AHM is illustrated in Scheme 1 (see Supporting Information (SI) for details). First, a tetraanthracenyl and dichloro-substituted oligophenylene **3** was synthesized by the Suzuki reaction of tetrabromo- and dichloro-substituted oligophenylene **1**[17,22] and 9-anthracene-boronic acid **2**, in 89% yield. Compound **3** was further reacted with *N*-*n*-hexadecyl maleimide through a Diels−Alder cycloaddition, yielding a dichloro-substituted oligophenylene monomer **4** with four AHM edge groups (86% yield). The successful synthesis of **3** and **4** was demonstrated by ^{1}H and ^{13}C nuclear magnetic resonance (NMR), matrix-assisted laser desorption/ionization time-of-flight (MALDI-TOF) mass, and elemental analyses (Figures S2−S7 and Pages S7−S11). Second, laterally expanded poly-*para*-phenylene precursor with AHM edge substituents (PPP-AHM) was synthesized by AA-type Yamamoto polymerization of monomer **4**. Recycling gel permeation chromatography (GPC) yielded three PPP-AHM samples (PPP-AHM-1, 2, and 3) with number-average molecular weights (M_ns) ranging from 13,000 to 124,000 and polydispersity indices (PDI) of 1.2−1.5 (determined by GPC, see Figure S12). Finally, through intramolecular oxidative cyclodehydrogenation in CH_2Cl_2 using $FeCl_3$ as the Lewis acid and oxidant, PPP-AHMs were converted into arm-chair edged GNR-AHMs with uniform width (1.7 nm) and different lengths. Since PPP-AHM-1, 2, and 3 possess 4, 8, and 42 repeating units (1.38 nm/unit), calculated from their M_ns, the corresponding average lengths of GNR-AHM-1, 2, and 3 are 6, 11, and 58 nm, respectively.

Fourier transform infrared spectra demonstrate the efficient "graphitization" and planarization of PPP into GNR (Figures S14−S16). In the spectra of GNR-AHMs the signals attributable to the aromatic C−H stretching vibrations and the out-of-plane (*opla*) C−H deformation are significantly attenuated compared with those of PPP-AHMs, while typical *opla* bands for aromatic C−H at the armchair edge of the GNR basal plane appear.[13,16,23] Solid-state NMR analyses prove that the semiflexible polyphenylene precursor becomes rigid and planar after "graphitization" (Figure S18).[13,16,17] Particularly, the 2D ^{1}H−^{1}H double quantum-single quantum (DQ-SQ) correlation spectra of PPPs exhibit narrow and resolved signals, whereas those of GNRs show broad, stretched, and split ridge signals in the aromatic region (Figures S18b,e). Moreover, the 2D ^{1}H−^{1}H DQ-SQ spectra display cross peaks that originate from the close spatial proximity of the two types of aromatic protons at the edge of the GNRs (Figure S18e), confirming the efficient planarization. The almost unchanged ^{13}C{^{1}H} CP/MAS NMR spectra indicate that the AHM groups are unaffected by the cyclodehydrogenation reaction (Figure S18c,f).

The first-order Raman spectra of the resulting GNRs exhibit typical D and G peaks (Figure 1a), as observed in other reported

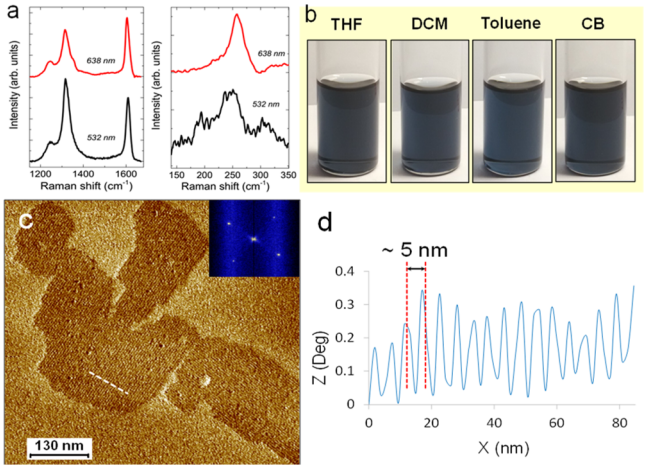

Figure 1. (a) Raman spectra of GNR-AHM-3, excited at 532 and 638 nm. (b) Pictures of GNR-AHM-3 in various solvents (0.1 mg mL^{-1}, see Figure S21 for 5 mg mL^{-1} dispersions). (c) AFM phase image of self-assembled domains of the GNRs on HOPG, with the corresponding fast Fourier transform (FFT) shown in the inset. Each set of two points (one point and its central inversion) in the FFT corresponds to a periodicity of ~5 nm along one direction. The presence of two pairs of points comes from the existence of two domains with lamellar periodicity in two different directions. (d) Line profile along the white dotted line in (c).

bottom-up synthesized GNRs.[13,16] The D band is not activated by defects, similarly to aromatic molecules, where the atomic vibrations of the D peak are Raman active.[24] The low-frequency region includes a characteristic peak at ~258 cm^{-1}, associated with the radial breathing-like layer mode (RBLM).[25] This is a fingerprint of narrow (<2 nm) and atomically precise GNRs.[26] The RBLM peak is more intense at 638 nm than 532 nm excitation, due to the electronic resonance.[25,26] By using the equation $w = 3222/\nu_{RBLM}$, where w is the width and ν_{RBLM} is the RBLM wavenumber, the estimated width is ~1.3 nm, in reasonable agreement with the structurally determined value (1.7 nm, Scheme 1).

Thanks to the bulky AHM, GNR-AHMs show superior dispersibility in organic solvents including THF, dichloromethane (DCM), toluene, and chlorobenzene (CB), among others (Figure 1b). Mild shaking or sonication of GNR-AHM in these solvents generates black homogeneous dispersions with concentrations of up to 5 mg mL^{-1} (Figures S20−S21), which were stable for over three months without precipitation. Such a dispersibility greatly surpasses those reported for alkylated GNRs (<0.05 mg mL^{-1} in THF), which require hours of ultrasonication and are stable for several days at most.[13,16,17] DLS analyses give similar unimodal narrow size distributions with average hydrodynamic diameters (D_h) of 40−60 nm for GNR-AHM-3 in the above-mentioned solvents with concentrations from 0.01 to 0.1 mg mL^{-1} (Figure S23). D_h being close to the length (~60 nm) of individual GNR-AHM-3 and not increasing with increasing concentration (0.01−0.1 mg mL^{-1}) suggests a single-ribbon character of the GNRs. Furthermore, GNR-AHMs can also be dispersed, albeit with more aggregation, in some polar solvents including *N*,*N*-dimethylformamide, dimethylsulfoxide, acetone, ethyl acetate, etc. (Figures S22−S23), which could not be achieved for the previously

DOI: 10.1021/jacs.8b06028
J. Am. Chem. Soc. 2018, 140, 10416−10420

reported alkyl-substituted or polymer-functionalized GNRs.[13,16,17]

Such excellent dispersibility allows drop-casting diluted dispersions of GNR-AHMs in 1,2,4-trichlorobenzene (TCB) on highly oriented pyrolytic graphite (HOPG). Self-assembled lamellae were imaged by AFM after solvent evaporation (Figures 1c and S24–S25). The domain sizes vary roughly from 10,000 to 250,000 nm^2, depending on the concentration. AFM topographies reveal uniform ~0.4 nm thick lamellae (Figure S25), demonstrating their monolayer feature. The self-assembled monolayers exhibit the same internal lateral periodicity of 5.0 ± 0.4 nm (Figure 1d), which is compatible with the width of a single GNR-AHM. The perfect lamellar order and the uniformity in periodicity of the monolayers demonstrate the homogeneity in shape and width of the GNRs. Moreover, the longitudinal sizes (45–500 nm) of the lamellae are larger than the length of single GNRs, indicating an end-to-end alignment fashion of the GNRs in addition to lateral side-by-side arrangement. The GNRs appeared as organized lamellae most likely because of van der Waals interactions among the alkyl chains. The self-assembly behavior on the surface is similar to those of alkyl-substituted GNRs, but film preparation is much simpler, not requiring strong ultrasonication needed in previous work.[13,16,17]

The absorption spectra of GNR-AHM-1 and 3 are very similar and contrast those of the previously reported poly(ethylene oxide)-functionalized GNRs (GNR-PEO) (Figure 2a).[17] While

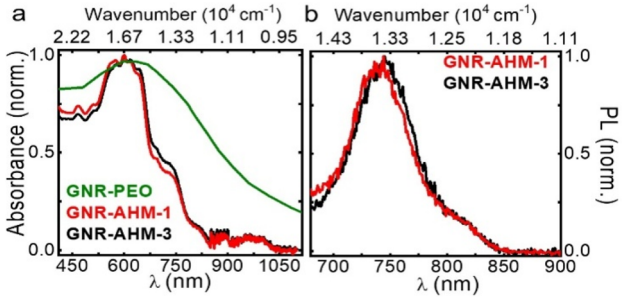

Figure 2. Absorption (a) and PL (b) spectra of GNR-AHMs in THF (0.03 and 0.003 mg mL^{-1} for absorption and PL measurements, respectively). GNR-PEO spectrum is reproduced from ref 17.

GNR-PEO shows featureless absorption in the visible with a long tail extending to the near-infrared (NIR) due to scattering, a typical sign of aggregation, GNR-AHMs have intense absorption limited to the region below 750 nm (weak absorption at 850–1000 nm is due to few aggregates, see Figure S31). There is almost perfect agreement between the absorption and photoluminescence (PL) (Figure 2b) of GNR-AHM-1 and 3, both being red-shifted compared to the monomer (Figure S11). Thus, the exciton is delocalized over no more than four monomer units for this edge structure. The optical bandgaps of GNR-AHMs are estimated to be ~1.69 eV by considering the lowest energy peak of PL and TA at ~735 nm. A linear relationship between PL intensity and concentration (<0.1 mg mL^{-1}) further confirms the single-ribbon character (Figure S26). GNR-AHM-3 exhibits a 9.1% PL quantum yield and PL lifetime of 8.7 ns (Table S1); these values could not be measured for other reported structurally defined GNRs due to aggregation-induced PL quenching.

Ultrafast TA experiments using 100 fs, 730 nm pump pulses were performed on GNR-AHM-1 and 3, giving similar results. Figure 3a summarizes the TA spectra of GNR-AHM-3 (see Figure S28 for GNR-AHM-1). Unlike the absorption (Figure

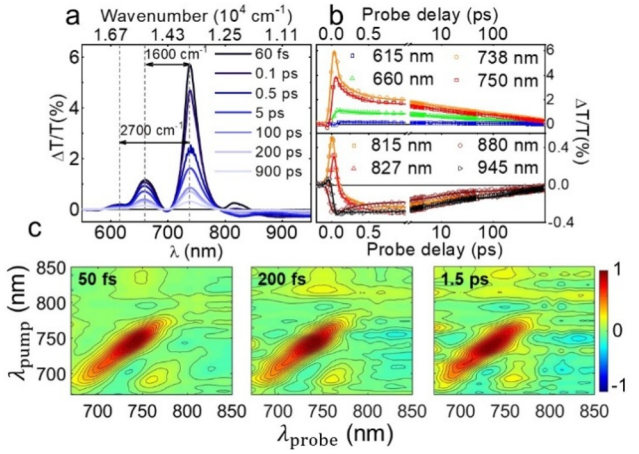

Figure 3. (a) TA spectra of GNR-AHM-3 (0.5 mg mL^{-1}) for different delays. (b) TA at specific wavelengths (symbols) with corresponding fits (solid lines). (c) Normalized NIR 2DES maps (2 mg mL^{-1}) at t_2 = 50, 200, and 1500 fs.

2a), the TA spectra are remarkably simple, consisting of three positive peaks at 738, 660, and 615 nm. At 660 and 615 nm, only ground state bleach (GSB) features are present, while GSB and stimulated emission (SE) signals exist at 738 nm. The separation between these peaks (Figure 3a) matches the G and 2D Raman peaks (Figure 1a). At early delay times, we observe a positive peak around 820 nm corresponding to SE from the lowest energy exciton to G and D vibrational replicas in the ground state. Therefore, even the 58 nm long GNR-AHM-3 behaves like a small organic molecule in solution, with the electronic structure of a vibronic progression.

Typical TA timetraces (Figure 3b) show an important 250 fs decay at 738 and 820 nm (containing SE signals), which is only weakly present at the other bands (see SI for global fit).[27] An accompanying broadening of the 738 band (Figure S32) suggests it is due to relaxation in the first excited state manifold. Two slower decay components of 9 and 290 ps are present equally in all bands, being similar to reported decays on small graphene molecules and carbon nanotubes.[28] As expected for molecules of this size, no rotational reorientation was observed.[29]

Finally, the nature of the lowest electronic transition is investigated with two-dimensional electronic spectroscopy (2DES) using ~10 fs NIR pulses.[30] 2DES gives a correlation map between pump and probe wavelengths (λ_{pump}, λ_{probe}) for each waiting time t_2 between them.[31] Figure 3c displays 2DES maps of GNR-AHM-3 at t_2 = 50, 200, and 1500 fs; the main feature is a peak stretched along the diagonal ($\lambda_{pump} = \lambda_{probe}$) with a cross peak parallel to it below the diagonal. Their separation of ~1350 cm^{-1} indicates that the main peak consists of two bands, with the short wavelength one being a vibronic replica. The remaining diagonal elongation marks inhomogeneous broadening, implying that different microscopic environments shift otherwise narrow absorption lines of individual chromophores.[32] As the waiting time increases, solvent fluctuations usually lead molecules to probe different environments, eventually resulting in a round line shape.[33] However, the main peak remains stretched even at 1.5 ps and TA spectra show no major broadening up to 900 ps (Figure S32). This suggests a

DOI: 10.1021/jacs.8b06028
J. Am. Chem. Soc. 2018, 140, 10416–10420

rigid but diverse range of microscopic structures around the GNRs, likely related to the AHM side groups.

In summary, we report grafting of bulky side groups at the edge of structurally defined GNRs, affording breakthrough in dispersion of GNRs. This allows us to study the electronic structure and optical properties of single ribbons. As synthetic methods toward GNRs with other edge structures are achieved, this approach can again be used to dissolve individual ribbons of other architectures, such as cove- or partially zigzag-edged ones. Control over the electronic and optical properties of GNRs with a single-ribbon feature holds promise in many potential applications, including field-effect transistor devices, light harvesting, fluorescence imaging, and photothermal conversion.

■ ASSOCIATED CONTENT

Supporting Information

The Supporting Information is available free of charge on the ACS Publications website at DOI: 10.1021/jacs.8b06028.

Experiments, supporting figures, and calculations (PDF)

■ AUTHOR INFORMATION

Corresponding Authors

*mai@sjtu.edu.cn (Y.M.)

*giulio.cerullo@fisi.polimi.it (G.C.)

ORCID

Tetsuhiko Nagahara: 0000-0003-1405-5515

Joan Teyssandier: 0000-0003-4369-0542

Michael Ryan Hansen: 0000-0001-7114-8051

Steven De Feyter: 0000-0002-0909-9292

Klaus Müllen: 0000-0001-6630-8786

Xinliang Feng: 0000-0003-3885-2703

Giulio Cerullo: 0000-0002-9534-2702

Yiyong Mai: 0000-0002-6373-2597

Author Contributions

¶Y.H. and F.X. contributed equally.

Notes

The authors declare no competing financial interest.

■ ACKNOWLEDGMENTS

The authors thank the financial support from National Natural Science Foundation of China (21320102006, 21774076, 51573091, and 91527304), Program of the Shanghai Committee of Science and Technology (17JC1403200), EC under Graphene Flagship (CNECT-ICT-604391 and 785219 GrapheneCore 2), ERC under the European Union's Horizon 2020 research and innovation program (648417), EPSRC in the framework of the CDT Graphene NOWNANO, and the National Physical Laboratory of London.

■ REFERENCES

(1) Nguyen, G. D.; Tsai, H.-Z.; Omrani, A. A.; Marangoni, T.; Wu, M.; Rizzo, D. J.; Rodgers, G. F.; R Cloke, R. R.; Durr, A.; Sakai, Y.; Liou, F.; Aikawa, A. S.; Chelikowsky, J. R.; Louie, S. G.; Fischer, F. R.; Crommie, M. F. *Nat. Nanotechnol.* **2017**, *12*, 1077.

(2) Cai, J.; Ruffieux, P.; Jaafar, R.; Bieri, M.; Braun, T.; Blankenburg, S.; Muoth, M.; Seitsonen, A. P.; Saleh, M.; Feng, X.; Müllen, K.; Fasel, R. *Nature* **2010**, *466*, 470.

(3) Cai, J.; Pignedoli, C. A.; Feng, X.; Müllen, K.; Fasel, R. *Nat. Nanotechnol.* **2014**, *9*, 896.

(4) Chen, Y. C.; Cao, T.; Chen, C.; Pedramrazi, Z.; Haberer, D.; Oteyza, D. G.; Fischer, F. R.; Louie, S. G.; Crommie, M. F. *Nat. Nanotechnol.* **2015**, *10*, 156.

(5) Kawai, S.; Saito, S.; Osumi, S.; Yamaguchi, S.; Foster, A. S.; Spijker, P.; Meyer, E. *Nat. Commun.* **2015**, *6*, 8098.

(6) Ruffieux, P.; Wang, S.; Yang, B.; Sánchez-Sánchez, C.; Liu, J.; Dienel, T.; Talirz, L.; Shinde, P.; Pignedoli, C. A.; Passerone, D.; Dumslaff, T.; Feng, X.; Müllen, K.; Fasel, R. *Nature* **2016**, *531*, 489.

(7) Wang, S.; Talirz, L.; Pignedoli, C. A.; Feng, X.; Müllen, K.; Fasel, R.; Ruffieux, P. *Nat. Commun.* **2016**, *7*, 11507.

(8) Jordan, R. S.; Li, Y. L.; Lin, C.; McCurdy, R. D.; Lin, J. B.; Brosmer, J. L.; Marsh, K. L.; Khan, S. I.; Houk, K. N.; Kaner, R. B.; Rubin, Y. *J. Am. Chem. Soc.* **2017**, *139*, 15878.

(9) Yang, X.; Dou, X.; Rouhanipour, A.; Zhi, L.; Müllen, K. *J. Am. Chem. Soc.* **2008**, *130*, 4216.

(10) Jänsch, D.; Ivanov, I.; Zagranyarski, Y.; Duznovic, I.; Baumgarten, M.; Turchinovich, D.; Li, C.; Bonn, M.; Müllen, K. *Chem. - Eur. J.* **2017**, *23*, 4870.

(11) Schwab, M. G.; Narita, A.; Hernandez, Y.; Balandina, T.; Mali, K. S.; Feyter, S. D.; Feng, X.; Müllen, K. *J. Am. Chem. Soc.* **2012**, *134*, 18169.

(12) Vo, T. H.; Shekhirev, M.; Kunkel, D. A.; Morton, M. D.; Berglund, E.; Kong, L.; Wilson, P. M.; Dowben, P. A.; Enders, A.; Sinitskii, A. *Nat. Commun.* **2014**, *5*, 3189.

(13) Narita, A.; Verzhbitskiy, I. A.; Frederickx, W.; Mali, K. S.; Jensen, S. A.; Hansen, M. R.; Bonn, M.; Feyter, S. D.; Casiraghi, C.; Feng, X.; Müllen, K. *ACS Nano* **2014**, *8*, 11622.

(14) Gao, J.; Uribe-Romo, F. J.; Saathoff, J. D.; Arslan, H.; Crick, C. R.; Hein, S. J.; Itin, B.; Clancy, P.; Dichtel, W. R.; Loo, Y. L. *ACS Nano* **2016**, *10*, 4847.

(15) Yang, W.; Lucotti, A.; Tommasini, M.; Chalifoux, W. A. *J. Am. Chem. Soc.* **2016**, *138*, 9137.

(16) Narita, A.; Feng, X.; Hernandez, Y.; Jensen, S. A.; Bonn, M.; Yang, H.; Verzhbitskiy, I. A.; Casiraghi, C.; Hansen, M. R.; Koch, A. H. R.; Fytas, G.; Ivasenko, O.; Li, B.; Mali, K. S.; Balandina, T.; Mahesh, S.; Feyter, S. D.; Müllen, K. *Nat. Chem.* **2014**, *6*, 126.

(17) Huang, Y.; Mai, Y.; Beser, U.; Teyssandier, J.; Velpula, G.; Van Gorp, H.; Straasø, L. A.; Hansen, M. R.; Rizzo, D.; Casiraghi, C.; Yang, R.; Zhang, G.; Wu, D.; Zhang, F.; Yan, D.; Feyter, S. D.; Müllen, K.; Feng, X. *J. Am. Chem. Soc.* **2016**, *138*, 10136.

(18) (a) Ezawa, M. *Phys. Rev. B: Condens. Matter Mater. Phys.* **2006**, *73*, 045432. (b) Osella, S.; Narita, A.; Schwab, M. G.; Hernandez, Y.; Feng, X.; Müllen, K.; Beljonne, D. *ACS Nano* **2012**, *6*, 5539. (c) Ivanov, I.; Yunbin, H.; Osella, S.; Beser, U.; Wang, H. I.; Beljonne, D.; Narita, A.; Müllen, K.; Turchinovich, D.; Bonn, M. *J. Am. Chem. Soc.* **2017**, *139*, 7982.

(19) Huang, Y.; Dou, W.-T.; Xu, F.; Ru, H.-B.; Gong, Q.; Wu, D.; Yan, D.; Tian, H.; He, X.-P.; Mai, Y.; Feng, X. *Angew. Chem., Int. Ed.* **2018**, *57*, 3366.

(20) Xu, Y.; Bai, H.; Lu, G.; Li, C.; Shi, G. *J. Am. Chem. Soc.* **2008**, *130*, 5856.

(21) Ramanathan, T.; Abdala, A. A.; Stankovich, S.; Dikin, D. A.; Herrera-Alonso, M.; Piner, R. D.; Adamson, D. H.; Schniepp, H. C.; Chen, X.; Ruoff, R. S.; Nguyen, S. T.; Aksay, I. A.; Prud'homme, R. K.; Brinson, L. C. *Nat. Nanotechnol.* **2008**, *3*, 327.

(22) (a) Huang, Y.; Mai, Y.; Yang, X.; Beser, U.; Liu, J.; Zhang, F.; Yan, D.; Müllen, K.; Feng, X. *J. Am. Chem. Soc.* **2015**, *137*, 11602. (b) Huang, Y.; Yuan, R.; Xu, F.; Mai, Y.; Feng, X.; Yan, D. *Polym. Chem.* **2016**, *7*, 1234.

(23) Centrone, A.; Brambilla, L.; Renouard, T.; Gherghel, L.; Mathis, C.; Müllen, K.; Zerbi, G. *Carbon* **2005**, *43*, 1593.

(24) Castiglioni, C.; Tommasini, M.; Zerbi, G. *Philos. Trans. R. Soc., A* **2004**, *362*, 2425.

(25) Zhou, J.; Dong, J. *Appl. Phys. Lett.* **2007**, *91*, 173108.

(26) Verzhbitskiy, I. A.; Corato, M. D.; Ruini, A.; Molinari, E.; Narita, A.; Hu, Y.; Schwab, M. G.; Bruna, M.; Yoon, D.; Milana, S.; Feng, X.; Müllen, K.; Ferrari, A. C.; Casiraghi, C.; Prezzi, D. *Nano Lett.* **2016**, *16*, 3442.

(27) Snellenburg, J. J.; Laptenok, S. P.; Seger, R.; Müllen, K. M.; van Stokkum, I. H. M. *J. Stat. Softw.* **2012**, *49*, 1.

(28) (a) Soavi, G.; Dal Conte, S.; Manzoni, C.; Viola, D.; Narita, A.; Hu, Y.; Feng, X.; Hohenester, U.; Molinari, E.; Prezzi, D.; Müllen, K.;

DOI: 10.1021/jacs.8b06028
J. Am. Chem. Soc. 2018, 140, 10416−10420

Cerullo, G. *Nat. Commun.* **2017**, *7*, 11010. (b) Paternò, G. M.; Chen, Q.; Wang, X.-Y.; Liu, J.; Motti, S. G.; Petrozza, A.; Feng, X.; Lanzani, G.; Müllen, K.; Narita, A.; Scotognella, F. *Angew. Chem., Int. Ed.* **2017**, *56*, 6753.
(29) Camargo, F. V. A.; Anderson, H. L.; Meech, S. R.; Heisler, I. A. *J. Phys. Chem. B* **2015**, *119*, 14660.
(30) Maiuri, M.; Réhault, J.; Carey, A.-M.; Hacking, K.; Garavelli, M.; Lüer, L.; Polli, D.; Cogdell, R. J.; Cerullo, G. *J. Chem. Phys.* **2015**, *142*, 212433.
(31) (a) Jonas, D. M. *Annu. Rev. Phys. Chem.* **2003**, *54*, 425. (b) Nuernberger, P.; Ruetzel, S.; Brixner, T. *Angew. Chem., Int. Ed.* **2015**, *54*, 11368.
(32) Hamm, P.; Zanni, M. *Concepts and Methods of 2D Infrared Spectroscopy*; Cambridge University Press: Cambridge, U.K., 2011.
(33) (a) Sanda, F.; Perlík, V.; Lincoln, C. N.; Hauer, J. *J. Phys. Chem. A* **2015**, *119*, 10893. (b) Moca, R.; Meech, S. R.; Heisler, I. A. *J. Phys. Chem. B* **2015**, *119*, 8623.

DOI: 10.1021/jacs.8b06028
J. Am. Chem. Soc. 2018, 140, 10416−10420